Microstructural Analyses of Cr(VI) Speciation in Chromite Ore Processing Residue (COPR)

MARIA CHRYSOCHOOU,*,†
SIRINE C. FAKRA,‡
MATTHEW A. MARCUS,‡
DEOK HYUN MOON,§ AND
DIMITRIS DERMATAS§

Department of Civil and Environmental Engineering, University of Connecticut, Storrs, Connecticut 06269, Advanced Light Source, Lawrence Berkeley National Lab, Berkeley, California, and Stevens Institute of Technology, Hoboken, New Jersey

Received February 18, 2009. Revised manuscript received May 27, 2009. Accepted May 31, 2009.

The speciation and distribution of Cr(VI) in the solid phase was investigated for two types of chromite ore processing residue (COPR) found at two deposition sites in the United States: gray-black (GB) granular and hard brown (HB) cemented COPR. COPR chemistry and mineralogy were investigated using micro-X-ray absorption spectroscopy and micro-X-ray diffraction, complemented by laboratory analyses. GB COPR contained 30% of its total Cr(VI) (6000 mg/kg) as large crystals (>20 μm diameter) of a previously unreported Na-rich analog of calcium aluminum chromate hydrates. These Cr(VI)-rich phases are thought to be vulnerable to reductive and pH treatments. More than 50% of the Cr(VI) was located within nodules, not easily accessible to dissolved reductants, and bound to Fe-rich hydrogarnet, hydrotalcite, and possibly brucite. These phases are stable over a large pH range, thus harder to dissolve. Brownmillerite was also likely associated with physical entrapment of Cr(VI) in the interior of nodules. HB COPR contained no Cr(VI)-rich phases; all Cr(VI) was diffuse within the nodules and absent from the cementing matrix, with hydrogarnet and hydrotalcite being the main Cr(VI) binding phases. Treatment of HB COPR is challenging in terms of dissolving the acidity-resistant, inaccessible Cr(VI) compounds; the same applies to ~50% of Cr(VI) in GB COPR.

Introduction

Chromite ore processing residue (COPR) was generated in the U.S. in millions of tons and widely used as wetland backfill and foundation material due to its sand-like properties. Three plants employing the high-lime roasting process were located in Hudson County, New Jersey and deposited approximately 2.75 million tons of COPR in the period 1905−1976. COPR has a residual chromium content of up to 50,000 mg/kg total chromium, half of which may occur as carcinogenic Cr(VI). Dermatas et al. (*1*), Wazne et al. (*2*), and Moon et al. (*3*) presented results of the remediation studies at SA7, a COPR deposition site in Jersey City, NJ. Efforts to treat COPR found at other sites across North America and the United Kingdom are also underway (*4*−*7*).

Remediation attempts using reductants such as ferrous sulfate ($FeSO_4$) and calcium polysulfide (CaS_5) only managed to decrease solid-bound Cr(VI) to 1000−2000 mg/kg, as determined by X-ray absorption near edge structure (XANES) spectroscopy, despite the high stoichiometric dosages (from 2× up to 8×) used in the treatability studies (*1, 3*). Reoxidation of Cr(III) was excluded as a mechanism for high residual Cr(VI), as manganese oxides, the only common materials that can oxidize Cr(III) (*8*), are not present in sufficient quantities in COPR. Hence, the only plausible explanation for treatment failure was that much of the Cr(VI) was not released from the solid and therefore not accessible to reductants. This conclusion is corroborated by parallel investigations, which showed that substantial amounts of Cr(VI) were bound within the COPR particles and thus recalcitrant to acid treatment (*7*).

COPR is a cementitious waste with primary constituents brownmillerite (Ca_2FeAlO_5) and periclase (MgO), which hydrate in aqueous alkaline environments. Chrysochoou and Dermatas (*9*) reported the presence of calcium aluminum chromium oxides hydrates (CAC) in COPR with the chemical formula $Ca_4Al_2(CrO_4)(OH)_{12}\cdot nH_2O$ (n = 3, 6, 8). CACs accounted for 50% on average (25−75% range) of the total Cr(VI). Hillier et al. (*10, 11*) reported that hydrogarnet ($Ca_3Al_2(OH)_{12}$) was also an important host phase for chromate in COPR from Glasgow, Scotland. Hillier et al. (*10*) reported Cr(VI)-hydrocalumite as Cr(VI) host instead of CAC to account for the X-ray diffraction (XRD) peak at 7.9 Å. Hydrocalumite ($Ca_4Al_2Cl_2(OH)_{12}\cdot 6H_2O$) is isostructural with the CACs, with chloride instead of chromate. This phase shares several peaks with the hydrotalcite group ($Mg_6Al_2(CO_3)(OH)_{16}\cdot 4H_2O$), which was reported instead of hydrocalumite in SA7 COPR. All these phases fall under the layered double hydroxides (LDH) or anionic clays. LDH have the same layered structure (Figure S1), consisting of brucite-like sheets, held together by anions and water molecules. LDH are capable of multiple cationic and anionic substitutions (*12*). Goswamee et al. (*13*) showed that a variety of LDH phases (Mg−Al, Ni−Al) could incorporate chromate in their structure. Thus, the chemical composition of an LDH structure that produces an XRD peak at 7.9 Å in COPR can vary (with Ca, Mg, Al, and Fe in the octahedral sheet and chloride, carbonate, or chromate in the interlayer). Ca−Al phases tend to be stable at higher pH values (>11), while Mg−Al phases are stable down to pH 8 or lower (*12*). The original pH of COPR is in the range 11.5−12.5, so that pH reduction is necessary to dissolve Cr(VI)-bearing phases. A Ca−Al LDH phase will require less acidity than Mg-bearing phases to dissolve bound Cr(VI). Thus, resolving which phases account for the observed peak at 7.9 Å and how they bind to chromate affect treatment considerations. The distribution and crystal size of Cr(VI)-bearing phases are also of engineering significance. This study presents results of synchrotron-based micro X-ray fluorescence (μXRF), μXANES spectroscopy, and μXRD analyses on COPR that were performed to investigate these issues.

Materials and Methods

Two types of COPR material were analyzed: the first one, obtained from SA7, was a gray-black (GB) granular material representative of largely unhydrated COPR. A second type, a reddish brown cemented material (denoted as HB), was obtained from Dundalk Marine Terminal, a COPR deposition site in Baltimore, MD.

TABLE 1. Bulk Chemistry and Mineralogy of GB and HB Samples (All Data except pH in wt.%)[a]

	GB	HB
pH	12.5	12.0
Cr(VI)	0.65	0.87
Cr	1.35	2.33
Ca	18.8	20.6
Fe	7.4	12.5
Al	3.3	5.5
Mg	6.4	4.6
brownmillerite	23.0	n.d.
periclase	3.0	n.d.
hydrogarnet	6.0	YES
brucite	7.6	YES
CAC (total)	3.1	YES
hydrotalcite	5.5	YES
calcite	6.2	n.d.
quartz	4.5	n.d.
ettringite	2.2	n.d.
amorphous	38.5	YES

[a] YES: observed but quantitative analysis was not performed due to preferred orientation effects. n.d.: not detected.

Chemical, bulk X-ray diffraction, and SEM/EDX methods are provided in Supporting Information. Representative samples were prepared as 30-μm-thick diamond-polished thin sections by Spectrum Petrographics (Vancouver, WA) for microprobe analyses. Micro XRF, μXRD, and μXANES measurements were performed on beamline 10.3.2 at the Advanced Light Source (ALS) (*14*). Micro-XRF elemental maps were acquired at 10 keV incident energy with a beam size of 7×7 μm^2 and a counting time of 50 ms/pixel. Fluorescence counts were collected for Ca, Ti, Cr, Mn, Fe, Ni, Cu, and Zn with a seven-element Ge solid-state detector. From elemental distribution maps, various spots of interest were selected for μXRD to identify crystalline phases and for Cr K-edge μXANES to probe Cr redox state. Cr chemical mapping was performed at incident energies of 5960, 5993, and 6250 eV to obtain the background, Cr(VI), and total Cr (Cr(tot)) signals, respectively. Energy calibration was performed using a Cr foil (5989.02 eV) (*15*). The background map was subtracted from the two others to obtain signals attributable to Cr only. Next, 7% of the Cr(tot) signal was subtracted from that of Cr(VI) to account for the finite XANES signal that Cr(III) species typically exhibit at the Cr(VI) energy. The Cr(VI) and Cr(tot) maps were then assembled into a composite map.

All μXANES spectra were collected in fluorescence mode, pre-edge background subtracted, and post-edge normalized using custom LabView software.

Microdiffraction patterns were recorded in transmission mode with a Bruker Smart6000 CCD camera at 17 keV for 5 min with a beam size of 16×7 μm^2. Two-dimensional patterns were radially integrated and calibrated using the Fit2d software (*16*) and an α-alumina standard.

Complementary μXRD measurements were performed in reflection mode on the GB thin section at ALS beamline 12.3.2 (*17*). Micro-XRF maps were first acquired, using a single element Si-drift detector, then μXRD was performed on Cr regions of interest using a MAR133 CCD camera oriented 90° to a 7 keV incident beam with spot size 10×2.5 μm^2. XRD patterns were processed with custom IDL software (XMAS) and calibrated with a silicon crystal. All one-dimensional XRD profiles were analyzed using Jade 8.5 (see Supporting Information).

Results

Bulk Chemistry and Mineralogy. The COPR samples had similar chemical composition (Table 1). Both contained significant amounts of Cr(VI) and Cr(III), with HB exhibiting higher total Cr concentration. The major elements in both samples were Ca, Fe, Al, and Mg, reflecting the lime addition and composition of chromite ore.

Three potential Cr(VI) sinks were identified: CAC, hydrotalcite (HT), and hydrogarnet (HG) (Table 1 and Figure S2). In GB, the amount of CAC was estimated at approximately 3 wt.%, accounting for 2360 mg/kg Cr(VI) or 35% of the total Cr(VI). Ettringite ($Ca_6Al_2(SO_4)_3(OH)_{12}\cdot 26H_2O$) is a cementitious mineral that can, theoretically, act as a Cr(VI) host. Chrysochoou and Dermatas (*9*) reported the presence of ettringite in SA7 COPR as pure sulfate species, with negligible chromate substitution. Hillier et al. (*10*) did, however, observe up to 50% chromate substitution in ettringite crystals in Glasgow COPR.

The HB XRD pattern (Figure S2) revealed no detectable parent minerals (brownmillerite, periclase) and brucite ($Mg(OH)_2$) was the only other phase except the three Cr(VI) sinks. Accurate quantification on this sample was prohibited by significant broadening and preferred orientation of the HT peaks.

Microstructural Analyses. Cr(VI) and Cr(tot) maps (Figure 1) were obtained in two areas of the GB thin section, denoted as GB1 (4×2.5 mm^2) and GB2 (5×2.5 mm^2), and one area of the HB sample (6.5×3.5 mm^2). A higher density of Cr(VI) compounds was observed in GB1, while the total Cr distribution and intensity was the same in both areas. By contrast, HB displayed about twice as many total Cr counts as GB and a widespread Cr(VI) distribution with fewer Cr(VI) concentrated spots. This is reflected in the distribution of the pixel intensities (Figure S4). GB and HB had the same distribution for about 50% of the pixels, which account for 17% of the total counts, while differences were observed at the upper fifth percentile. The top 1% of the pixels accounts for approximately 10% of the total counts in GB and 4% for HB.

In GB, high-Cr(VI) crystals (or crystal assemblages) were quite large with quasi-circular spots >50 μm in diameter (above 70% of the maximum intensity) and elongated spots at least 70 μm long and 30 μm wide. The largest Cr(VI)-rich area (100×100 μm^2) was observed in GB1. Significant differences in Cr(VI) spatial distribution were also observed. Figure 2 shows Ca and Cr(VI) distributions in the two samples. Ca is the most abundant element in COPR and its presence is considered most representative of solid COPR, given that the microprobe at BL10.3.2 cannot detect lighter elements like Mg and Al. HB consisted of round Cr(VI)-binding nodules interconnected with a Ca-rich matrix corresponding to a mixture of hydrated cementitious compounds, lending HB COPR its cementing properties. Surprisingly, this matrix contained no Cr(VI), which was only concentrated within the nodules. In GB, the cementing matrix between nodules existed to a more limited extent, consistent with its unhydrated and loose granular nature. Cr(VI) was distributed both in the nodules and in the diffuse cementing material. Tinjum et al. (*6*) observed similar Cr distribution in GB COPR (without differentiation of the species), i.e. as both surface contaminant and diffuse within nodules.

For XANES analyses, Cr(VI) spots of various intensities were targeted to capture a large range of Cr(VI)-binding compounds. None of the XANES spectra (Figure 3) matched any available standards for Cr(VI) (K_2CrO_4, Na_2CrO_4, $CaCrO_4$, or $PbCrO_4$), despite the presence of a pre-edge peak at 5993 eV in most spots. This was expected, as Cr(VI) is bound to chemically complex cementitious compounds, whose synthesis and analysis as pure compounds for linear combination fitting was not possible. However, GB and HB exhibited some common features (e.g., nodes at 6030 and 6050 eV) that could

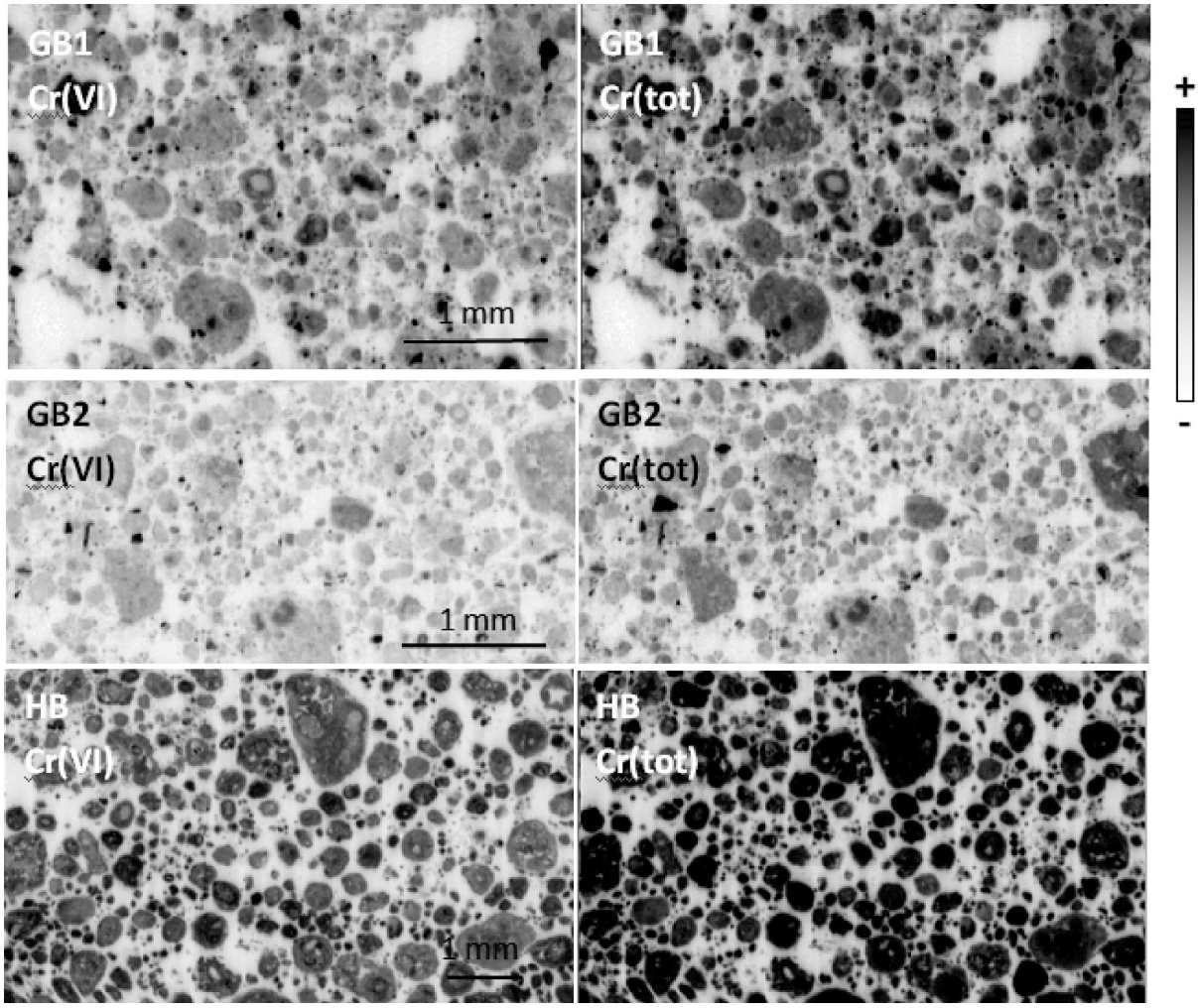

FIGURE 1. Cr(VI) and Cr(tot) μXRF maps of GB1, GB2, and HB areas.

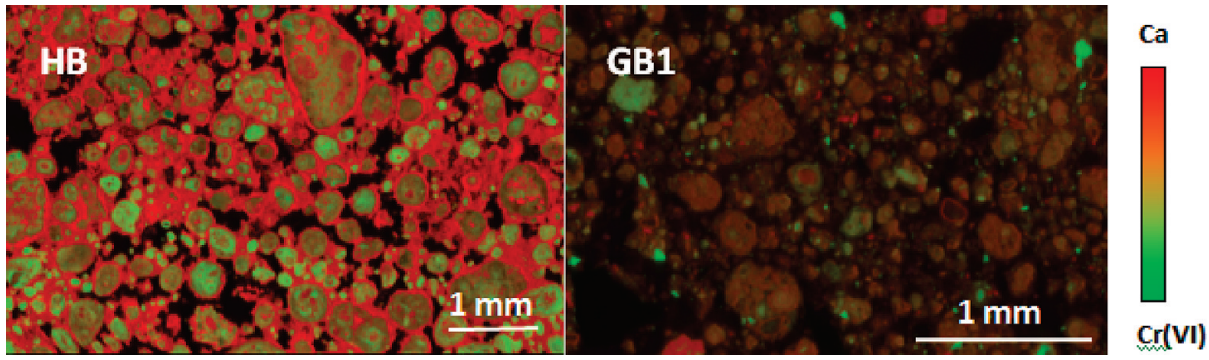

FIGURE 2. Bicolor coded μXRF maps showing Ca (in red) and Cr(VI) (green) distributions in COPR HB and GB1 areas.

be attributed to structurally similar compounds. To overcome the lack of appropriate standards, two approaches were adopted:

(a) Principal Component Analysis (PCA) (*18*) was performed in abstract mode to determine the number of components needed to model the XANES spectra and to investigate similarities in the relative abundance of abstract components between different spots.

(b) Micro-XRD and SEM/EDX analyses were conducted to identify the chemistry and mineralogy of the spots.

PCA Results. Four spots corresponded to chromite and were excluded from the data set; 43 spectra remained. The IND values were minimized at 12 components, indicating that XANES spectra were modeled best by using 12 different species. However, relatively good fittings (<1% residual) could be obtained using the first three eigenvectors or abstract components. Since three vectors could be projected onto 2-D space, the respective weights were used for further analysis. The components were denoted as $comp_{i=0-2}$, as they did not correspond to actual Cr(VI) species. The 43 spots were categorized into five groups (Figure 4), which were related to the amount of Cr(VI) retained in the structure. The pre-edge peak height (PEPH) at 5993 eV ranged from 1 to 0.4 in clusters 1 to 5, respectively. The similarity in the post-edge region also points to structural similarities within each group. XRD and SEM/EDX results for each cluster are summarized in Table 2.

Cluster 1. All ten spots of cluster 1 with the maximum Cr(VI) PEPH (1.0) belonged to GB. Eight spots displayed similar XRD and SEM/EDX spectra (Figures S4, S5 and Table

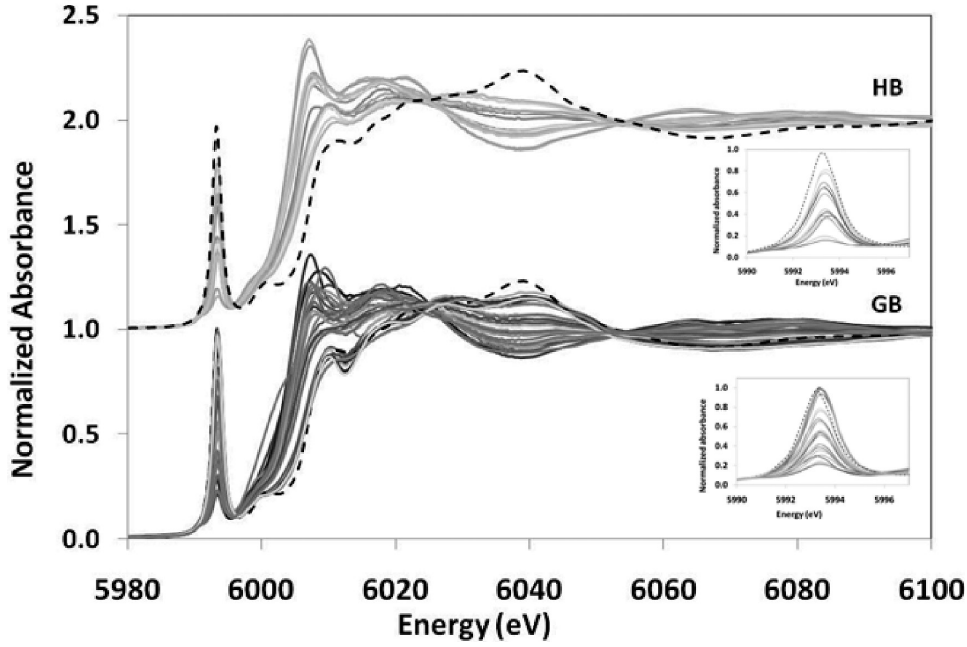

FIGURE 3. XANES spectra of COPR HB spots (top) and GB spots (bottom). The inserts show the characteristic Cr(VI) pre-edge peak at 5993 eV. K_2CrO_4 spectrum (dash line) is shown as a reference.

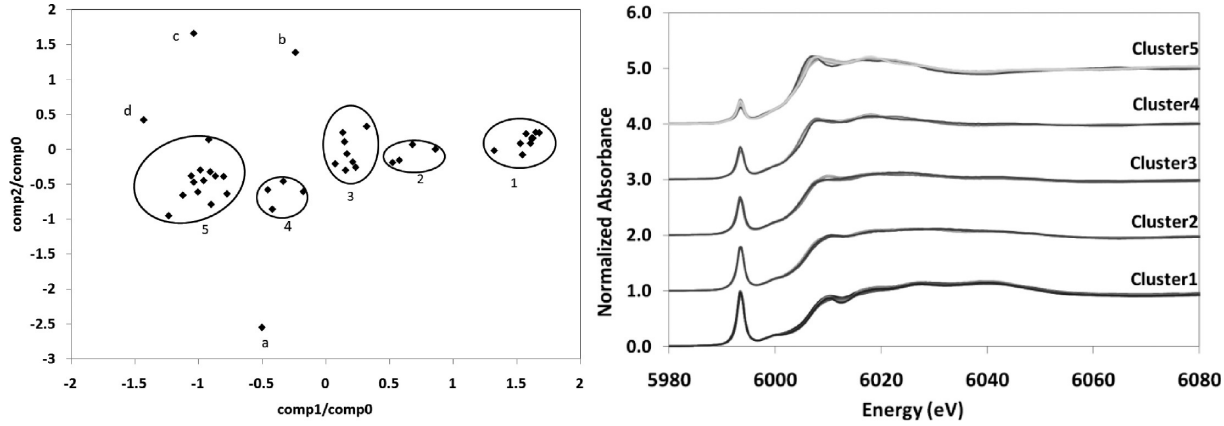

FIGURE 4. Plot of the relative weights of the first three eigenvectors for 43 Cr spots (left) and corresponding XANES spectra (right); circles denote clusters.

S1). Prominent XRD peaks matched PDF 44-0272 ($NaCa_4Al_2O_6(SO_4)_{1.5}\cdot 15H_2O$) and PDF41-0478 ($Ca_4Al_2O_6(CrO_4)\cdot 12H_2O$). SEM revealed crystals with parallel cleavage typical of platy particles; the EDX approximately corresponded to $Na_{0.6}Ca_4Al_2O_6(CrO_4)_{1.3}(OH)_{12}\cdot xH_2O$, or a chromate analog of PDF 44-0272. Thus, incorporation of Na in CACs enables the accommodation of more chromate in the interlayer compared to the regular CAC. SEM analyses of multiple GB samples showed that crystals with parallel cleavage were frequently present, with crystal size ranging from 10 to 50 μm (Figure S5) (*19*). The remaining two spots in this cluster had Na-free CAC.

Cluster 2. The PEPH was the same in all four spots (~0.8), but small differences were observed in the postedge region. XRD patterns of GB spots showed relatively small CAC peaks, mixed with brownmillerite, periclase, brucite, and hydrogarnet. SEM/EDX analyses on these spots were inconclusive, indicating a mixture of compounds with Ca, Fe, Al, Mg, Cr, and Si. HB spots also contained hydrogarnet and CAC. Thus, either small (less than the 16 × 7 μm^2 beam size) CAC or hydrogarnet crystals could have produced the observed XANES spectra.

Cluster 3. The PEPH was approximately 0.7 on all spots. Three GB spots did not show a "kink" at 6010 eV when compared to the others. The only common phase among these three spots was brownmillerite (Table S2), but EDX showed that Ca/Al and Fe/Al ratios were not always consistent with the brownmillerite stoichiometry. Direct incorporation of Cr(VI) into brownmillerite-like structures has been previously observed by Gibb (*20*), emerging as a possible mechanism for Cr(VI) binding in the COPR matrix. The location of these spots (Figure S6) could also indicate the physical chromate incorporation into either brownmillerite grains or amorphous Fe-rich hydration products that locally surround brownmillerite grains in the interior of nodules. The remaining spots of cluster 3 contained hydrogarnet, brucite, and goethite (α-FeOOH). The μXRF map of one spot (Figure S7) showed that Cr(VI), Cr(III), Ca, and Fe coexisted in the 7 × 7 μm^2 pixel, with significant variation in their relative abundance within a small distance. It is therefore likely that the microbeam resolution was inadequate in this case to capture the heterogeneity of COPR mineralogy. Whether the Cr(VI) mechanism is that of physical or chemical inclusion in the brownmillerite structure, the location of this fraction is such that its release into solution is likely to be extremely slow.

The ubiquitous presence of brucite and iron oxyhydroxides in XRD patterns of cluster 3 spots suggests a potential

TABLE 2. Overview of μXRD and SEM/EDX Results for the 5 PCA Clusters[a]

	GB spots	HB spots
cluster 1	10 spots with maximum (1.0) PEPH 8 spots Na- and Cr-rich CAC $Na_{0.6}Ca_4Al_2O_6(CrO_4)_{1.3}(OH)_{12}\cdot xH_2O$ 1 spot Si-rich CAC, 1 spot CAC	no spots in this group
cluster 2	2 spots with PEPH 0.8 CAC, hydrogarnet	2 spots with PEPH 0.8 CAC, hydrogarnet
cluster 3	4 spots with PEPH 0.7 3 spots with no "kink" at 6010 eV and brownmillerite 1 spot hydrogarnet, brucite, goethite	4 spots with PEPH 0.7 3 spots hydrogarnet, hydrotalcite, brucite, goethite 1 spot all of the above plus CAC
cluster 4	3 spots with PEPH 0.6 1 spot brucite only 1 spot hydrotalcite, brucite, hydrogarnet 1 spot brucite, hydrogarnet	1 spot with PEPH 0.6 hydrotalcite, brucite, hydrogarnet
cluster 5	5 spots with PEPH 0.3−0.4 brucite in all spots goethite brownmillerite barite	7 spots with PEPH 0.3−0.4 hydrotalcite, hydrogarnet
stray spots	A: mostly brucite B: Si-rich katoite C: brucite D: brownmillerite, hydrotalcite	

[a] All phases are listed in order of apparent quantity in μXRD patterns.

role of these phases in binding Cr(VI). Comparison of the XANES spectra with the reference spectrum of Cr(VI) sorbed on goethite (*21*) showed no resemblance with any of the spectra in cluster 3 (Figure S8) or any other group so that sorption is not considered a predominant mechanism at the high COPR pH. Ginder-Vogel et al. (*22*) found that Cr(VI) was bound to portlandite ($Ca(OH)_2$) grains, although they did not clarify the binding mechanism. It is therefore possible that structurally similar brucite and portlandite can bind Cr(VI), even though there is no direct evidence to this end.

Cluster 4. XRD and SEM/EDX results on cluster 4 spots (3 GB and one HB) were very similar to those of cluster 3. Mg was the predominant element detected via EDX. Brucite was identified in all spots by μXRD. Hydrogarnet was found in the GB spots, while hydrotalcite was dominant in two of them. A $20 \times 20\,\mu m^2$ μXRD map (Figures S9 and S10) obtained at BL12.3.2 around point GB2-12 indicated that the Cr(VI)-rich area had pronounced LDH (hydrocalumite or hydrotalcite) peaks, and EDX (Table S3) showed that the phase had both Ca and Mg in the octahedral layer. Brucite was also present in the surrounding pixels and thus may serve as an Mg source for the formation of Mg-rich LDH, rather than as direct Cr(VI) sink.

Cluster 5. Twelve spots comprised cluster 5, with five of them in GB. Seven out of fifteen spots in HB had a Cr(VI) PEPH between 0.3 and 0.4, forming the predominant group and confirming that Cr(VI) in HB was diffuse. HB spots had mineral assemblages similar to previous groups, where hydrotalcite and hydrogarnet prevailed, and with brucite and goethite as secondary minerals. No new phases were observed that could account for structural differences in Cr(VI) binding in HB COPR.

Stray Spots. No new Cr(VI)-binding phases were found associated with these stray spots (Table 2).

Discussion and Environmental Significance

There are both common features and significant differences between GB and HB COPR in terms of Cr(VI) speciation and distribution. GB contained large Cr(VI) hotspots of size varying between ~30 and 100 μm in diameter. SEM images revealed large crystals (>20 μm diameter) with characteristic basal cleavage, which correspond to a newly identified Na-rich form of calcium aluminum chromate hydrates (CAC) with the ability to retain more than 1 mol chromate per mol CAC. The approximate chemical formula is $Na_{0.6}Ca_4Al_2O_6(CrO_4)_{1.3}(OH)_{12}\cdot xH_2O$, with Na varying between 0.5 and 1 and chromate varying between 1.25 and 1.5. A Na- and Cr(VI)-rich analog of hydrogarnet was also observed. These Cr(VI)-rich compounds accounted for 30% of all analyzed spots, which agrees with the bulk XRD quantitative analysis. Given the size and location of these crystals, it is considered that the 30% Cr(VI)-rich fraction is easily accessible to treatment solutions (acidic and/or reductive) and thus amenable to treatment without requiring pH decrease below 10 or particle size reduction.

Phases with medium Cr(VI) in their structure (PEPH 0.6−0.8) made up approximately 20% of all GB spots. Hydrogarnet and small amounts of Na-free CAC were the predominant phases associated with this fraction. Brownmillerite also arose as a potential candidate to bind Cr(VI), with both chemical inclusion and physical entrapment as possible retention mechanisms. This fraction is located near the center of nodules that are not easily accessible to treatment agents.

The remaining spots with smaller amounts of Cr(VI) (PEPH < 0.5) were primarily associated with Mg- and Fe-rich phases, mainly hydrotalcite and Fe-rich hydrogarnet. Brucite could also potentially play a role in Cr(VI) immobilization in these spots, as it was ubiquitous and Cr(VI) binding by structurally similar portlandite ($Ca(OH)_2$) has been previously observed (*22*). In GB, these phases can be found both within the nodules and within the cementing matrix. The presence of Mg-rich phases is important for Cr(VI) release, given the fact that they are stable over a wider range of pH than Ca−Al-rich hydrogarnet and CACs. Geelhoed et al. (*23*), Chrysochoou (*19*), and Tinjum et al. (*6*) showed hydrotalcite and brucite peaks surviving down to pH 7 upon acid addition to COPR. Given that the majority of Cr(VI) (~50%) was associated with this fraction, it is concluded that to facilitate quick release of Cr(VI) from GB COPR, the addition of substantial amounts of acid and particle size reduction would likely be required. Alternatively, slow diffusion of Cr(VI) from the matrix would be expected, in which case a stepwise reductant addition and a long curing time would be necessary. These observations agree with the failure of various attempts to reduce solid Cr(VI) below 1000 mg/kg and the regulatory levels at this site (*1, 2, 6, 7*).

The HB sample appeared to have less differentiation between the types of structures binding Cr(VI). It contained no high-Cr(VI) binding phases, and only 15% of the spots analyzed had pre-edge peak heights over 0.5. Hydrogarnet, hydrotalcite, and brucite appeared in most XRD patterns, so that no real differentiation could be made on the ability of the three groups to bind higher or lower amounts of Cr(VI). Cr(VI) was generally diffuse within the matrix; more importantly Cr(VI) was not found in the cementing matrix connecting the nodules but only within the nodules. The combination of these observations indicates that Cr(VI) treatment in HB COPR would be even more challenging than for GB: the material is a lot more cemented and the cementation would have to be broken not only to facilitate

the addition of reductant, but also to access Cr(VI). Even then, accessing diffuse, nodule-bound Cr(VI) would not be easy. There are currently no studies in the literature on reductive treatment of HB COPR, which is found more as isolated layers within COPR sites, rather than as bulk material. However, the presence of this material is likely to complicate any in situ reductive treatment of COPR sites with HB layers.

Acknowledgments

This work was supported by the University of Connecticut Research Foundation. We thank M. Kunz and N. Tamura for support at ALS BL12.3.2. ALS-LBNL operations are supported by the Director, Office of Science, Office of Basic Energy Sciences, U.S. Department of Energy under contract DE-AC02-05CH11231.

Supporting Information Available

Section S1 provides detailed description of the XRD and SEM/EDX methods; Section S2 includes additional figures and tables that support the analyses of the five PCA clusters. This material is available free of charge via the Internet at http://pubs.acs.org.

Literature Cited

(1) Dermatas, D.; Chrysochoou, M.; Moon, D. H.; Grubb, D. G.; Wazne, M.; Christodoulatos, C. Ettringite-Induced Heave in Chromite Ore Processing Residue (COPR) upon Ferrous Sulfate Treatment. *Environ. Sci. Technol.* **2006**, *40* (18), 5786–5792.

(2) Wazne, M.; Jagupilla, S. C.; Moon, D. H.; Jagupilla, S. C.; Christodoulatos, C.; Kim, M. G. Assessment of calcium polysulfide for the remediation of hexavalent chromium in chromite ore processing residue (COPR). *J. Hazard. Mater.* **2007**, *143*, 620–628.

(3) Moon, D. H.; Wazne, M.; Jagupilla, S. C.; Christodoulatos, C.; Kim, M. G.; Koutsospyros, A. Particle size and pH effects on remediation of chromite ore processing residue (COPR) using calcium polysulfide (CaS_5). *Sci. Total Environ.* **2008**, *399*, 2–10.

(4) Graham, M. C.; Farmer, J. G.; Anderson, P.; Paterson, E.; Hillier, S.; Lumsdon, D. G.; Bewley, R. J. F. Calcium polysulfide remediation of hexavalent chromium contamination from chromite ore processing residue. *Sci. Total Environ.* **2006**, *364*, 32–44.

(5) Su, C.; Ludwig, R. D. Treatment of hexavalent chromium in chromite ore processing solid waste using a mixed reductant solution of ferrous sulfate and sodium dithionite. *Environ. Sci. Technol.* **2005**, *39*, 6208–6216.

(6) Tinjum, J. M.; Benson, C. H.; Edil, T. B. Treatment of Cr(VI) in COPR Using Ferrous Sulfate—Sulfuric Acid or Cationic Polysulfides. *J. Geotech. Geoenviron. Eng.* **2008**, *134* (12), 1791–1803.

(7) Tinjum, J. M.; Benson, C. H.; Edil, T. B. Mobilization of Cr(VI) in chromite ore processing residue through acid treatment. *Sci. Total Environ.* **2008**, *391*, 13–25.

(8) Manceau, A.; Charlet, L. X-ray absorption spectroscopic study of the sorption of Cr(III) at the oxide-water interface I. Molecular mechanism of Cr(III) oxidation on Mn oxides. *J. Colloid Interface Sci.* **1992**, *148*, 425–442.

(9) Chrysochoou, M.; Dermatas, D. Application of the Rietveld method to assess Cr(VI) speciation in Chromite Ore Processing Residue. *J. Hazard. Mater.* **2007**, *141* (2), 370–377.

(10) Hillier, S.; Roe, M. J.; Geelhoed, J. S.; Fraser, A. R.; Farmer, J. G.; Paterson, E. Role of quantitative mineralogical analysis in the investigation of sites contaminated by chromite ore processing residues. *Sci. Total Environ.* **2003**, *308*, 195–210.

(11) Hillier, S.; Lumsdon, D. G.; Brydson, R.; Paterson, E. Hydrogarnet: a host phase for Cr(VI) in Chromite Ore Processing Residue (COPR) and other high pH wastes. *Environ. Sci. Technol.* **2007**, *41*, 1921–1927.

(12) Prasanna, S. V.; Kamath, P. V.; Shivakumara, C. Synthesis and characterization of layered double hydroxides (LDH) with intercalated chromate ions. *Mater. Res. Bull.* **2007**, *42*, 1028–1039.

(13) Goswamee, R. L.; Sengupta, P.; Bhattacharyya, K. G.; Dutta, D. K. Adsorption of Cr(VI) in layered double hydroxides. *Appl. Clay Sci.* **1998**, *13*, 21–34.

(14) Marcus, M. A.; MacDowell, A. A.; Celestre, R.; Manceau, A.; Miller, T.; Padmore, H. A.; Sublett, R. E. Beamline 10.3.2 at ALS: a hard X-ray microprobe for environmental and materials sciences. *J. Synchrotron Radiat.* **2004**, *11*, 239–247.

(15) Kraft, S.; Stümpel, J.; Kuetgens, U. High resolution x-ray absorption spectroscopy with absolute energy calibration for the determination of absorption edge energies. *Rev. Sci. Instrum.* **1996**, *67* (3), 681–687.

(16) Hammersley, A. P. FIT2D V9.129 - Reference manual V3.1; Vol. 346; ESRF internal report ESRF98HA01T; Macquarie University, Sydney, 1998.

(17) Kunz, M.; Tamura, N.; Chen, K.; MacDowell, A. A.; Celestre, R. S.; Church, M. M.; Fakra, S.; Domning, E. E.; Glossinger, J. M.; Kirschman, J. L.; Morrison, G. Y.; Plate, D. W.; Smith, B. V.; Warwick, T.; Yashchuk, V.; Padmore, H. A.; Ustundag, E. A dedicated superbend X-ray microdiffraction beamline for materials-, geo- and environmental sciences at the Advanced Light Source. *J. Synchrotron Radiat. Rev. Sci. Instrum.* **2009**, *80* (3), 5108.

(18) Ressler, T.; Wong, J.; Roos, J.; Smith, I. Quantitative speciation of Mn-bearing particulates emitted from autos burning (methylcyclopentadienyl) manganese tricarbonyl-added gasolines using XANES spectroscopy. *Environ. Sci. Technol.* **2000**, *34*, 950–958.

(19) Chrysochoou M. Investigation of environmental and geotechnical implications associated with deposition of Chromite Ore Processing Residue (COPR); Ph. D. dissertation, Stevens Institute of Technology, Hoboken, NJ, 2006.

(20) Gibb, T. C. Study of calcium—chromium—iron oxides by extended X-ray absorption fine structure spectroscopy. *J. Mater. Chem.* **1992**, *2*, 105–110.

(21) Wilkin, R. T.; Su, C.; Ford, R. G.; Paul, C. J. Chromium removal processes during groundwater remediation by a zerovalent iron permeable reactive barrier. *Environ. Sci. Technol.* **2005**, *39* (12), 4599–4605.

(22) Ginder-Vogel, M.; Borch, T.; Mayes, M. A.; Jardine, P. M.; Fendorf, S. Chromate reduction and retention processes within arid subsurface environments. *Environ. Sci. Technol.* **2005**, *39*, 7833–7839.

(23) Geelhoed, J. S.; Meussen, C. L.; Hillier, S.; Lumsdon, D. G.; Thomas, R. P.; Farmer, J. G.; Paterson, E. Identification and geochemical modeling of processes controlling leaching of Cr(VI) and other major elements from chromite ore processing residue. *Geochim. Cosmochim. Acta* **2002**, *66* (22), 3927–3942 .